The Research Council of Norway (NFR)

NORSAR

NORSAR Scientific Report No. 1-96/97

Semiannual Technical Summary

1 April 1996 - 30 September 1996

Kjeller, November 1996

7.3 Tuning of processing parameters for Global Threshold Monitoring at the IDC

Introduction

Detailed presentations of the Global Threshold Monitoring System developed for the IDC have been given in several of the NORSAR Semiannual Technical Summaries (Kværna et al., 1994a; Kværna et al., 1994b; Ringdal et al., 1995). To optimize the overall performance of the system, we have in this reporting period focused on tuning of the processing parameters and the beam deployments for the different stations of the IMS primary network, see Fig. 7.3.1. This has been done by requesting event segments from the IDC followed by detailed analysis of several events for each of the stations.

Generic global attenuation and travel-time curves form the basis for the calculation of network magnitude thresholds. As is well known, the attenuation curves are accompanied with significant uncertainties. For example, studies made on P-wave amplitude variability (Veith and Clawson, 1972; Lilwall, 1986; Ringdal and Fyen, 1979) indicate a standard deviation of about 0.4 magnitude units. This uncertainty is, however, accounted for in the calculation of magnitude thresholds.

In order to obtain optimized and realistic magnitude thresholds there are also other uncertainty factors that need to be addressed. These are:

- The use of STA envelopes as a representation of log(A/T)
- The effect of beamforming, filtering and different instrument responses on the seismic amplitude
- The effect of each target point representing a finite geographical area, and mis-steering of the array beams

These factors will be addressed in the following where we present the results from the tuning of the array station ASAR (Alice Springs, Australia).

Event selection

For each station it is important to have available a data set that is representative for the different types of P-phases usually observed. For the assessment of seismic magnitude thresholds the most significant variables are the dominant signal frequencies, the signal loss due to beamforming and mis-steering of the beams, and the characteristics of the seismic noise field. The signal variables are usually strongly dependent on the source-receiver distance, and we have therefore decided to collect data from events located at different distance ranges. High SNR signals are needed for the assessment of signal loss due to mis-steering of the beams, and we have found that data from about 10 events would allow us to derive reasonably representative processing parameters. Information on the events used for tuning of ASAR are given in Table 7.3.1.

Prefiltering

For magnitude estimation at the IDC, a 3rd order Butterworth filter with a passband between 0.8 and 4.5 Hz is applied to the data prior to the estimation of the signal amplitude and period. To resemble the procedure used for m_b calculation at the IDC, we will also apply the same baseline filter to the data prior to the generation of STA envelopes. For some stations, this passband may, however, be contaminated by high noise amplitudes, e.g., due to local noise sources or to the broadband characteristics of the instrument.

Another factor to consider is the frequency content of the different kinds of signals (local, regional, teleseismic and core phases). We should also have in mind that the global P-wave attenuation relationship (e.g. Veith and Clawson, 1972) is derived from instruments with a peak response around 1 Hz, and that we do not know the validity of this relation for signals with high dominant frequencies, like many local and regional P-phases.

Our approach to a possible adjustment of the filter setting is that we will need very strong arguments to change the filter parameters.

Ideally we would like there to be a close correspondence between the most energetic frequency range of the signal and the frequency range providing the highest SNR. In this way we could prefilter the data in a passband that ensured both correct magnitude thresholds during event intervals as well as optimum performance during noise conditions. This is, however, not the usual situation for **ASAR**. A typical example is given in Fig. 7.3.2, where we have analyzed a P-phase from an event at a distance of 33.6 degrees. The highest SNR is found between 2 and 3 Hz, whereas the largest A/T value is measured between 1 and 1.5 Hz.

The same characteristics are also illustrated in Fig. 7.3.3, where we compare the dominant signal frequency measured on the filtered beams providing the highest SNR, with the dominant frequency used for the estimation of event magnitude. The data set is **ASAR** P-phase information given in the database associated with the IDC Reviewed Event Bulletin (REB) for the year 1996. This comparison clearly shows that the highest SNR is usually found at higher frequencies than those providing the largest A/T value. Also notice the absence of REB events located within 10 degrees of **ASAR**.

From analysis of the 10 **ASAR** events and the statistics shown in Fig. 7.3.3, we have found no strong arguments for changing the parameters of the prefilter. For the 10 events, we have also manually measured the maximum A/T on both unfiltered and filtered (0.8-4.5 Hz) data. Except for the largest event of m_b 5.6, the correspondence was good, and log(A/T) was on the average about 0.05 m_b units lower after prefiltering, see Fig. 7.3.4.

For the m_b 5.6 event, log(A/T) was measured 0.69 m_b units lower after prefiltering, indicating that the main signal energy is found below the lower cutoff. When looking at the narrowband log(A/T) measurements of Fig. 7.3.5, we clearly see this behavior where the largest A/T is measured at about 0.5 Hz. For estimation of event magnitudes, the 0.8-4.5 Hz prefiltering will obviously give rise to errors. But for threshold monitoring we are assessing the **upper** magnitude limit of possible seismic events that might have occurred in a given area, and are therefore almost always focusing on magnitude levels close to the

background noise level. For events at such magnitude levels, we do not expect signals to have the main energy below the lower cutoff of the filter. We therefore argue that even though large events may have the main energy below 0.8 Hz, this will have very little influence on the calculation of magnitude thresholds.

The use of STA envelopes as a representation of log(A/T)

If we assume that an instrument response is flat to velocity, and that the length of the short-term-average (STA) includes a full cycle of a sinusoidal signal, we have the following relation between the STA and the amplitude (A) and period (T) of the signal:

$$\frac{A}{T} = \frac{\pi}{2} \cdot calib \cdot STA \qquad (1)$$

where *calib* is the calibration constant at the reference period.

The continuous calculation of STA traces of filtered beams forms the basis for the calculation of magnitude thresholds. For the 10 **ASAR** events, we have in Fig. 7.3.6 compared the manually measured maximum A/T values with the corresponding values of STA, both measured on data bandpass filtered between 0.8 and 4.5 Hz. The STA length was 1 second. For this small data set there is good correspondence, and the log(A/T) values have a mean bias of 0.04 m_b units relative to the log(STA) values. This serves to confirm the validity of using the continuous STA traces as a basis for the calculation of magnitude thresholds.

Signal loss due to beamforming

As seen from Figs. 7.3.2 and 7.3.5, beamforming of **teleseismic** P-phases using the sensors of the **ASAR** array provide significant SNR improvement without significantly reducing the signal amplitudes, at least for frequencies below 2 Hz. For higher frequencies, signal decorrelation starts to cause reduction of the beam amplitudes. The signal loss referred to in the following is defined as:

$$\text{Signal loss} = \text{Beam STA} \,/\, \text{Average STA of the individual sensors} \qquad (2)$$

where the STA was taken to be the maximum within 8 seconds after the signal onset.

When calculating the total signal loss due to beamforming in the fairly wide 0.8 - 4.5 Hz frequency band, it is clear that this loss is dependent on the dominant frequency range of the signal. For teleseismic events, we generally expect that the higher frequencies have been attenuated such that the main signal energy is found at lower frequencies, which again would imply little signal loss. For local and regional events, see Fig. 7.3.7, the major signal energy is typically found above 2 Hz, and a higher signal loss is expected.

Due to the large variation in signal spectra, we can only operate with approximate a priori estimates of the signal loss, but it will be reasonable to categorize the expected signal loss into bins of source-receiver distances. Fig. 7.3.8 shows the signal loss due to beamforming of the 10 **ASAR** events. For distances above 30 degrees we find the signal loss to be within 0.5 dB, and for distances between 15 and 30 degrees a maximum signal loss of 3.2 dB is observed. For distances below 15 degrees we have so far no data, but for signals with dom-

inant frequencies approaching 4.5 Hz, we expect that signal losses up to 4 dB may be found for the full **ASAR** array configuration.

From this small data set it would be reasonable to set the expected signal loss for events above 30 degrees to about 0.3 dB. For distances between 15 and 30 degrees, the average is a bit less than 2 dB. Below 15 degrees we have no data, so we have to look for more data or use information from other arrays to obtain an estimate of the expected signal loss.

Beam deployment and signal loss due to mis-steering

When deploying a beam set for processing of array data, we often require the signal loss due to mis-steering of the beams to be less than a given value, e.g. 3 dB. If we know the approximate value of the slowness mis-steering (s/km) corresponding to the 3 dB signal loss, we can derive the steering parameters (azimuth and slowness) of the necessary beam deployment.

When analyzing the **ASAR** events, we have calculated the signal loss due to mis-steering for data filtered between 0.8 and 4.5 Hz. Fig 7.3.9 shows the steering points used in this analysis, with values relative to the observed slowness and azimuth of the event. Figs. 7.3.10 and 7.3.11 show two examples of signal loss plotted as a function of the absolute value of the mis-steering for two events at 15.9 and 33.6 degrees distance, respectively.

The expected signal loss due to mis-steering is dependent on the frequency range of the main signal energy, which again shows a strong dependency on the source-receiver distance. As previously suggested, we have categorized the data into two bins, one for the distance interval 15-30 degrees, and another for 30-180 degrees.

Fig. 7.3.12 gives the average signal loss curve for the 4 events in the distance interval 15-30 degrees. After smoothing, the signal loss for the correct beam steering is 1.56 dB, and additional 3 dB signal loss is found for a mis-steering of 0.036 s/km. In order to deploy beams for events in the distance interval 15-30 degrees, we find in the IASP91 travel-time table that we expect the slowness to fall within the range 8.85 s/deg. to 13.63 s/deg. For the purpose of deploying the minimum number of beams required to cover a given slowness area, we have developed a semi-automatic procedure. The result is shown in Fig. 7.3.13 where the area between the two bold circles represent the slowness range for the 15-30 degrees distance interval, now in units s/km. We initially found that complete coverage within the 3 dB level could be achieved with deployment of 12 beams, but by extending the beam deployment to 17 beams and moving the steering points to larger slowness, the same beams could also be used for monitoring the distance range 2-15 degrees. The radii of the small circles is 0.036 s/km, corresponding to the expected mis-steering associated with the 3 dB signal loss.

Fig. 7.3.14 gives the average signal loss curve for the 6 events in the distance interval 30-180 degrees. After smoothing, the signal loss for the correct beam steering is as low as 0.16 dB, and additional 3 dB signal loss is found for a mis-steering of 0.041 s/km. As seen from the figure there is some spread in the observations, and in particular one event is less sensitive to mis-steering, primarily due to low dominant signal frequencies. The standard deviation associated with the 3 dB level is about 0.1 m_b units. For the distance interval 30-

180 degrees we expect the slowness to fall within the range 0.0 - 8.85 s/deg, illustrated by the disc within the bold circle of Fig. 7.3.15. In order to ensure complete coverage within the 3 dB level (0.041 s/km), 7 beams were necessary, represented by the centers of the small circles.

For the distance interval below 15 degrees, we have so far no data in our tuning set. From analysis of local and regional events at the ILAR array (in Alaska, USA), which has approximately the same configuration as ASAR, we have found it reasonable to assume the signal loss to be 30% more sensitive to mis-steering than for events between 15 and 30 degrees, i.e., slowness associated with the 3 dB signal loss is reduced by 30% down to 0.025 s/km. If we exclude P-phases from surface events within 2 degrees, there is very little difference between the theoretical slowness at 2 and 15 degrees. The slowness range is from 13.63-13.75 s/deg., illustrated by the small area between the bold circles of Fig. 7.3.16. By using the same 17 beams as for the 15-30 degrees interval, but now with smaller 3 dB circles, we see from Fig. 7.3.16 that complete coverage is ensured for the 2-15 degrees slowness interval.

Geographical grid spacing and time/azimuth/slowness tolerances

In our current implementation of the Threshold Monitoring system we have divided the Earth's surface into 2562 grid points, where each grid point covers a target area with a radius of about 2.7 degrees. In threshold monitoring there is a trade-off between the size of the target area and the tolerances of the parameter values used in the threshold computations. With a given grid, it is necessary to make the tolerances of each aiming point compatible with the grid spacing. An illustration of the need for introducing azimuth tolerances is given in Fig. 7.3.17, now for a global grid system with 162 points. From this figure we can see that the necessary azimuth tolerance will increase with decreasing distance to the aiming point.

If we are deploying a beam with a slowness and azimuth corresponding to the coordinates of the center of a target area, it is necessary to allow for some mis-steering such that every point within the target area is covered. We have in Fig. 7.3.18.a plotted the calculated maximum mis-steering (s/km) for each of the 2562 grid points, versus the distance to the grid points. When comparing the maximum mis-steering of each target region with the signal loss for events between 30 and 180 degrees (Fig. 7.3.14), we find that the mis-steering associated with the grid spacing cause much less than 1 dB signal loss. In the legend of Fig. 7.3.18a we have given the station-target distances where we find that the mis-steering associated with the grid spacing cause 1, 3, 5, 7 and 9 dB signal loss when using the relation between signal loss and mis-steering representative for events between 30 and 180 degrees.

In Fig. 7.3.18.b we have done the same calculations, but now for events between 15 and 30 degrees. The relation between signal loss and mis-steering for events between 15 and 30 degrees is given in Fig. 7.3 12. From the legend of Fig. 7.3.18.b we read that the mis-steering introduced to cover the target regions will correspond to 1 dB signal loss at a station-target distance of 17 degrees, and about 1.5 dB at 15 degrees.

As previously outlined, we have no data for the distance interval below 15 degrees, but if we assume that the signal loss for events between 2 and 15 degrees is 30% more sensitive to mis-steering than events between 15 and 30 degrees, we get the numbers given in the legend of Fig. 7.18.c. This tells us that we need to compensate for a signal loss of 3 dB at 13.3 degrees, 5 dB at 9.87 degrees, 7 dB at 7.9 degrees and 9 dB at 6.6 degrees. If we look at the beamforming SNR improvement of the event at 15.9 degrees distance (Fig. 7.3.7), we find a gain of about 9 dB. For events at closer distances than 15.9 degrees we do not expect this number to increase. This would imply that for distances within 6-7 degrees, the signal loss attributed to the mis-steering needed to cover the target regions (9 dB) will cancel the SNR improvement (9 dB) gained through beamforming.

Under the assumption that the 2-15 degrees model for the relation between signal loss and mis-steering is reasonable, we would for targets within about 7 degrees distance use the STA traces from a single array channel as the basis for calculating magnitude thresholds. When using a single array channel, the problem of signal loss vanishes, and there is no need to take into account such effects in the processing. For target distances closer than 7 degrees, the use of STA traces from a single channel would give better performance than using STAs from a beam based on the full **ASAR** configuration.

An alternative to using the data from a single channel, would be to use a smaller sub-configuration of the **ASAR** array for beamforming. In this way the signal loss would become less sensitive to mis-steering, and it could make sense to use STAs from beams also for a distance interval within 7 degrees. Such a decision would also have to take into account the fact that fewer array sensors provide less SNR improvement by beamforming.

Conclusions

When estimating the processing parameters for a given station for use in the Threshold Monitoring system, there are a couple of principles that we should have in mind:

- We want to be conservative with respect to estimating the upper magnitude thresholds, such that we should avoid using too optimistic values.
- At the same time we should be aware that the generic global attenuation relationship has an attributed uncertainty of about 0.4 m_b units, and that using average parameter estimates with an associated uncertainty of, e.g., 0.05 m_b units has little influence on the overall performance of the system.

We will in the following summarize the findings from the tuning analysis of the ASAR array:

- *Prefiltering*
  There seems to be no problem with the 0.8-4.5 Hz prefiltering of the ASAR array data, see Fig. 7.3.4. After excluding the large m_b 5.6 event, we did observe an average reduction in the estimated log(A/T) values of 0.05 m_b units after prefiltering. This should be taken into account in the parametrization of ASAR.

- *The relation between log(A/T) and log(π/2*calib*STA)*
  There is good correspondence between the manual signal measurements of log(A/T) and the automatic estimates of log(π/2*calib*STA) when measured on 0.8-4.5 Hz pre-filtered data, see Fig. 7.3.6. The automatic STA measurement had a small reduction of 0.04 m_b units relative to the manual A/T measurement, and this will be accounted for in the parametrization.

- *Signal loss by beamforming*
  For teleseismic events we found very little reduction in the signal amplitudes when beamforming with steering delays corresponding to the estimated azimuth and slowness of the observed P-phases, and as seen from Fig. 7.3.8, an average value of 0.25 dB was found.
  In the distance range 15-30 degrees, the average signal loss for the 4 events was 1.7 dB, but there was a relatively large scatter in the observations. In order to be conservative with the estimation of magnitude thresholds, we will increase this number to 2.5 dB in the parametrization.
  For the distance interval 7-15 degrees, we have no data in our tuning set, but from experience with analysis of ILAR events, we will increase the expected signal loss in the 15-30 degree distance range by 30%, such that the number becomes 3.25 dB.
  For the distance range within 7 degrees, we will derive the magnitude thresholds from a single array channel, and we will therefore have no signal loss due to beamforming.

- *Signal loss by mis-steering of the beams*
  Average curves for the relation between mis-steering of the beams and the reduction of signal amplitude are given in Fig.7.3.12 (15-30 degrees) and in Fig.7.3.14 (30-180 degrees). These will be used in the processing of the ASAR data.
  For the distance interval 7-15 degrees, we use the curve for the 15-30 degrees distance range, but increase the sensitivity to mis-steering by 30%.
  The problem of mis-steering is avoided for the distance range within 7 degrees where we use data from a single array channel

- *Beam deployment*
  Plots of the beam deployments for the different distance ranges are given in Figs. 7.3.13, 7.3.15 and 7.3.16. Details on the beamforming steering parameters are summarized in Table 7.3.2

With the information provided above at hand, the program for calculation of network magnitude thresholds will automatically include additional variables like the STA sampling rate, size of the target regions and the distribution of the beam deployment.

For quality control of the ASAR processing parametrization we plan to inspect a few time intervals with magnitude thresholds based on ASAR data alone, and check that the results are in agreement with general seismological knowledge.

We have in this contribution discussed in great detail the different aspects of the tuning process of the ASAR array for use in the Global Threshold Monitoring system at the IDC.

For tuning of the remaining stations of the IDC primary network, we plan to present only the final results as outlined above in this chapter.

T. Kværna

References

Kværna, T., F. Ringdal, H. Iversen and N.H.K. Larsen (1994a): A system for continuous global seismic threshold monitoring, *Semiann. Tech. Summary, 1 Oct 1993 - 31 Mar 1994,* NORSAR Sci. Rep, 2-93/94, NORSAR, Kjeller, Norway.

Kværna, T., F. Ringdal, H. Iversen and N.H.K. Larsen (1994b): A system for continuous seismic threshold monitoring, final report, *Semiann. Tech. Summary, 1 Apr - 30 Sep 1994,* NORSAR Sci. Rep, 1-94/95, NORSAR, Kjeller, Norway.

Lilwall (1986): Empirical amplitude-distance / depth curves for short-period P waves in the distance range 20-180°, AWRE Report No. O 30/86.

Ringdal, F. and J. Fyen (1979): Analysis of Global P-wave Attenuation Characteristics using ISC data files, *Semiann.Tech. Summary 1 Apr - 30 Sep 1979*, NORSAR Sci. Rep. 1-79/80, NORSAR, Kjeller, Norway.

Ringdal, F., T. Kværna and S. Mykkeltveit (1995): Global seismic threshold monitoring and automated network processing, *Semiann. Tech. Summary, 1 Oct 1994 - 31 Mar 1995,* NORSAR Sci. Rep, 2-94/95, NORSAR, Kjeller, Norway.

Veith, K. F. and G. E. Clawson (1972): Magnitude from short-period P-wave data, *Bull. Seism. Soc. Am.*, 62, 435-453.

Table 7.3.1. Information on the 10 events used for tuning for the Threshold Monitoring Parameters at the ASAR array.

Station	Orid	Lat	Lon	Depth	Origin time	Ndef	M_b	Delta	Phase	SNR	Azim	Vel
ASAR	808519	-12.8037	121.5608	0.0	1996:263:11.44.08.5	12	4.3	15.930	Pn	111.91	310.65	9.2
ASAR	808685	-6.0600	128.9550	321.2	1996:263:18.45.07.5	15	3.5	18.142	P	291.60	347.64	9.7
ASAR	808530	-4.0314	135.6428	0.0	1996:263:12.17.34.0	12	4.4	19.593	P	224.45	7.20	10.3
ASAR	817516	0.9085	126.7151	25.8	1996:273:09.00.45.2	48	4.8	25.408	P	114.15	343.33	18.2
ASAR	808621	-19.6428	169.8287	0.0	1996:263:14.04.38.2	14	4.4	33.573	P	249.52	86.78	12.5
ASAR	808505	-25.3101	179.8348	487.3	1996:263:21.05.28.6	50	4.3	41.676	P	394.12	95.32	14.2
ASAR	815191	-17.5973	-178.8668	626.8	1996:271:16.47.43.8	9	3.5	44.455	P	602.50	87.28	13.2
ASAR	817504	51.6327	161.2944	26.6	1996:272:17.07.05.4	50	4.7	78.740	P	208.29	16.79	20.2
ASAR	809239	-52.9173	9.8323	0.0	1996:264:17.37.05.8	38	5.6	89.622	P	40.08	205.56	24.3
ASAR	805509	11.5426	-85.3205	194.0	1996:262:17.34.22.2	75	5.0	140.847	PKhKP	67.30	107.20	34.8

Table 7.3.2. Information on the ASAR beam deployment used for global threshold monitoring.

No	Distance range	Type	Config	Vel	Azi	3dB	Filter
1	0-7	Single	AS12	-	-	-	0.8-4.5
2	7-15	Beam	ASAR	8.96	0.0	0.025	0.8-4.5
	15-30	-	-	-	-	0.036	0.8-4.5
3	7-15	Beam	ASAR	8.96	21.2	0.025	0.8-4.5
	15-30	-	-	-	-	0.036	0.8-4.5
4	7-15	Beam	ASAR	8.96	42.4	0.025	0.8-4.5
	15-30	-	-	-	-	0.036	0.8-4.5
5	7-15	Beam	ASAR	8.96	63.5	0.025	0.8-4.5
	15-30	-	-	-	-	0.036	0.8-4.5
6	7-15	Beam	ASAR	8.96	84.7	0.025	0.8-4.5
	15-30	-	-	-	-	0.036	0.8-4.5
7	7-15	Beam	ASAR	8.96	105.9	0.025	0.8-4.5
	15-30	-	-	-	-	0.036	0.8-4.5
8	7-15	Beam	ASAR	8.96	127.1	0.025	0.8-4.5
	15-30	-	-	-	-	0.036	0.8-4.5
9	7-15	Beam	ASAR	8.96	148.2	0.025	0.8-4.5
	15-30	-	-	-	-	0.036	0.8-4.5
10	7-15	Beam	ASAR	8.96	169.4	0.025	0.8-4.5
	15-30	-	-	-	-	0.036	0.8-4.5
11	7-15	Beam	ASAR	8.96	190.6	0.025	0.8-4.5
	15-30	-	-	-	-	0.036	0.8-4.5
12	7-15	Beam	ASAR	8.96	211.8	0.025	0.8-4.5
	15-30	-	-	-	-	0.036	0.8-4.5
13	7-15	Beam	ASAR	8.96	232.9	0.025	0.8-4.5
	15-30	-	-	-	-	0.036	0.8-4.5
14	7-15	Beam	ASAR	8.96	254.1	0.025	0.8-4.5
	15-30	-	-	-	-	0.036	0.8-4.5
15	7-15	Beam	ASAR	8.96	275.3	0.025	0.8-4.5
	15-30	-	-	-	-	0.036	0.8-4.5
16	7-15	Beam	ASAR	8.96	296.5	0.025	0.8-4.5
	15-30	-	-	-	-	0.036	0.8-4.5
17	7-15	Beam	ASAR	8.96	317.6	0.025	0.8-4.5
	15-30	-	-	-	-	0.036	0.8-4.5
18	7-15	Beam	ASAR	8.96	338.8	0.025	0.8-4.5
	15-30	-	-	-	-	0.036	0.8-4.5

No	Distance range	Type	Config	Vel	Azi	3dB	Filter
19	30-180	Beam	ASAR	13.58	26.6	0.041	0.8-4.5
20	30-180	Beam	ASAR	13.58	153.4	0.041	0.8-4.5
21	30-180	Beam	ASAR	13.58	206.6	0.041	0.8-4.5
22	30-180	Beam	ASAR	13.58	333.4	0.041	0.8-4.5
23	30-180	Beam	ASAR	15.18	90.0	0.041	0.8-4.5
24	30-180	Beam	ASAR	15.18	270.0	0.041	0.8-4.5
25	30-180	Beam	ASAR	Inf	0.0	0.041	0.8-4.5

The fields of the table are the following:

Distance range: Station-target distance range (in degrees) for which the STA data from the given beam should be used to derive the magnitude thresholds.

Type: Type of STA data to be used, a beam or a single channel.

Config: Configuration used for beamforming, or name of the single channel.

Vel: Apparent velocity of the beam.

Azi: Azimuth of the beam.

3dB: Expected mis-steering (in s/km) corresponding to 3 dB signal loss.

Filter: Prefilter applied to the data (3rd order Butterworth)

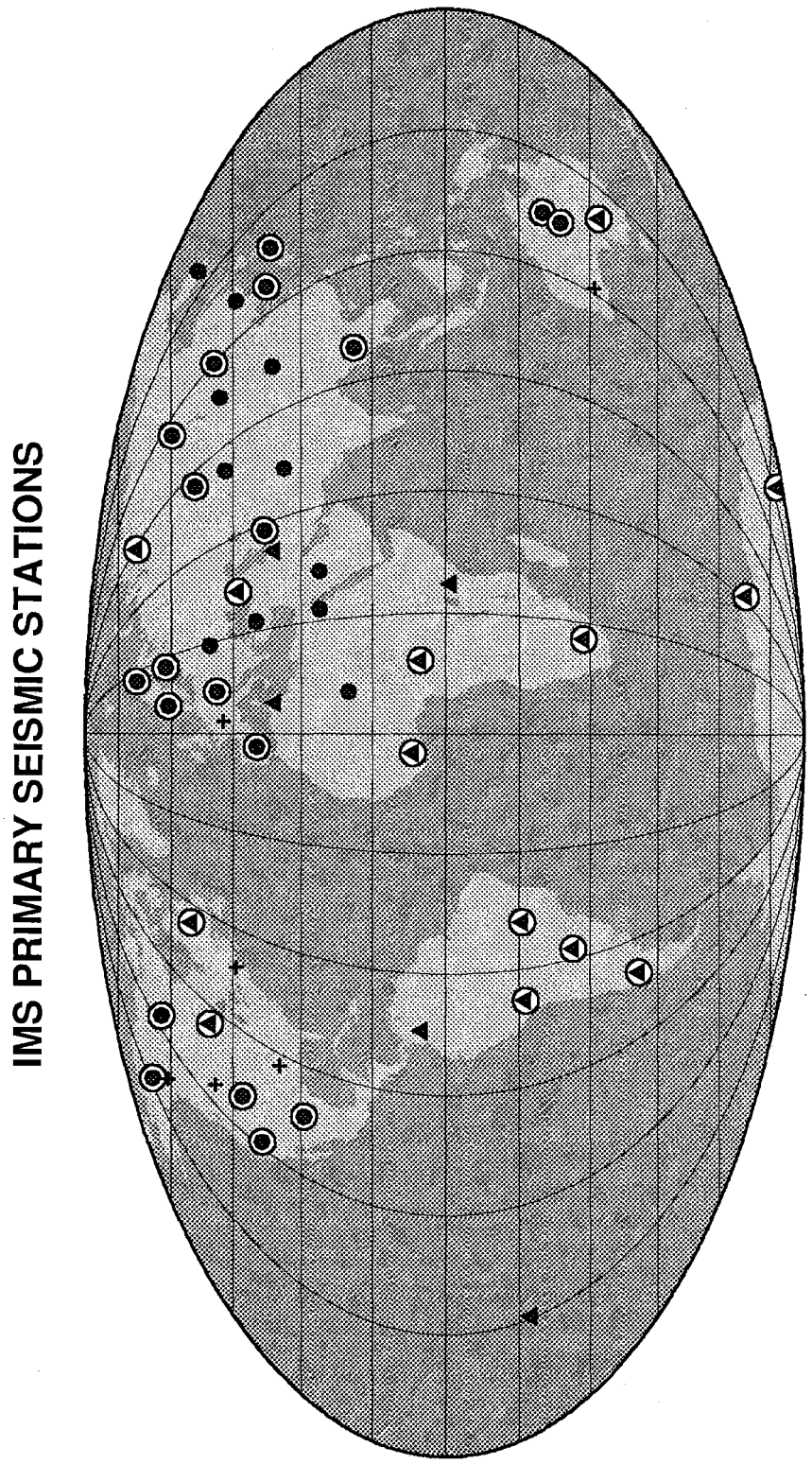

Fig. 7.3.1. Global map of the stations in the IMS primary network.

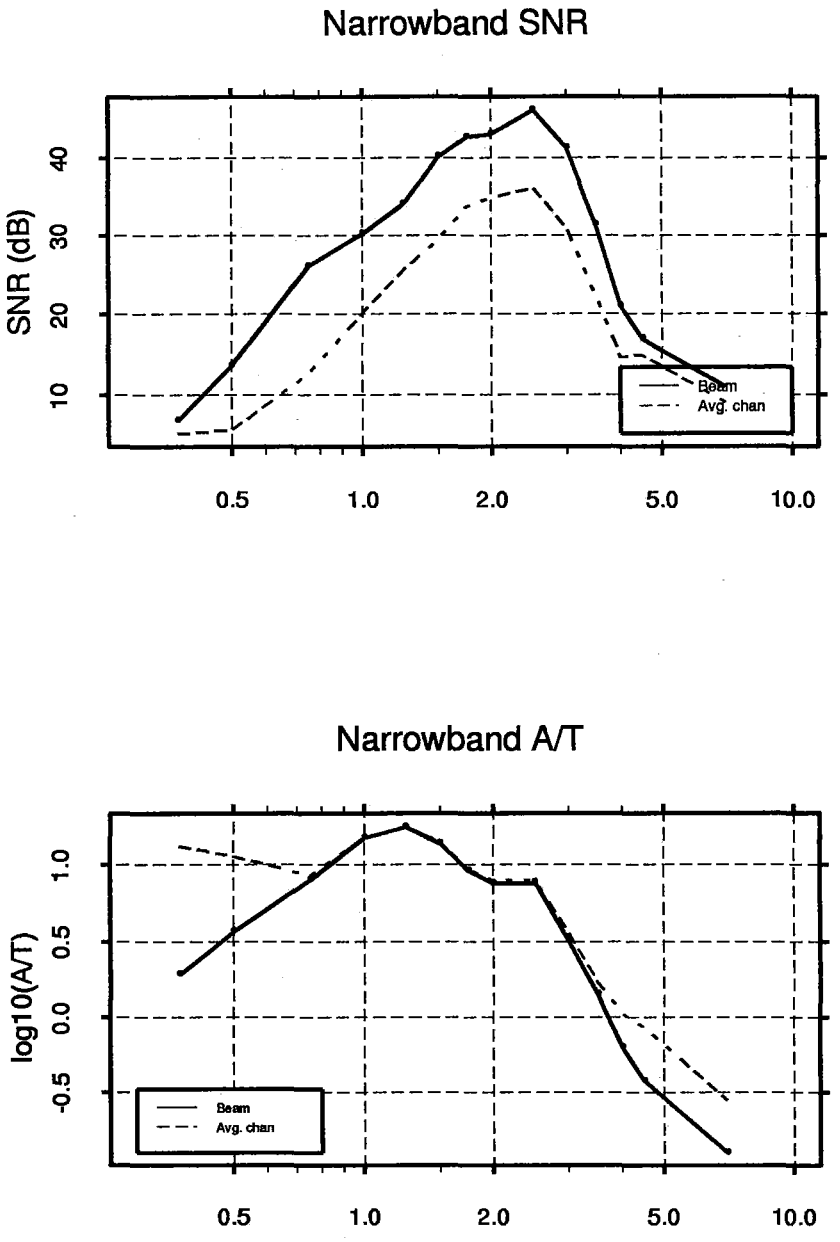

Fig. 7.3.2. The upper part of the figure shows the maximum SNR of the signal from an event at 33.6 degrees distance (no. 5 in Table 7.3.1) measured in a series of narrow filters, where the x-axis corresponds to the center of the filter bands.
The filters were the following given in Hz: 0.25-0.50, 0.25-0.75, 0.50-1.00, 0.75-1.25, 1.00-1.50, 1.25-1.75, 1.50-2.00, 1.75-2.25, 2.0-3.0, 2.5-3.5, 3.0-4.0, 3.5-4.5, 4.0-5.0, 6.0-8.0.
The solid line represents the SNR of the beam and the dashed line represents the average SNR of the array channels. The difference between the two curves can be interpreted as the SNR gain by beamforming.
The lower part of the figure shows the maximum A/T (nm/s) of the narrowband filtered data, measured within 8 seconds of the signal onset. Again the solid line represents the beam, and the dashed line represents the average of the array channels. For the part of the frequency range where the signal is above the background noise level, in this case above 0.75 Hz, the difference between the two curves can be interpreted as the signal loss by beamforming.

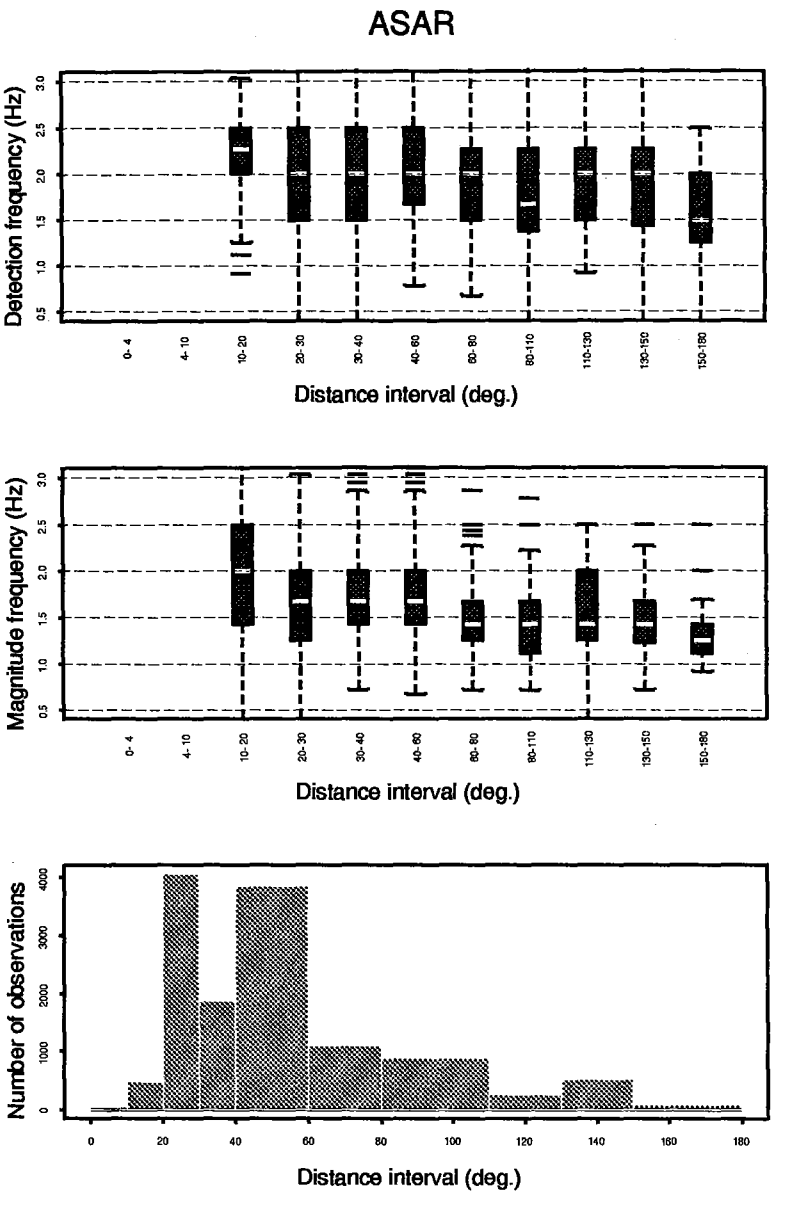

Fig. 7.3.3. The upper part of the figure shows the dominant signal frequencies measured on the filtered beams providing the highest SNR. The data set is **ASAR** *P-phase information given in the database associated with the IDC Reviewed Event Bulletin. For each distance bin, the box represents the span between the 1st and 3rd quartile of the data, and the line in the middle is plotted at the median value. The whiskers extend to 1.5*(inter quartile distance), and observations falling outside this range are given by separate lines. For each distance bin, this plot should thus give us an idea about the frequency range where we would expect the highest SNR.*

The middle part of the figure shows the same type of statistics, but now for the dominant frequencies used in the estimation of event magnitude. Notice that the array beams used in the estimation of m_b have been prefiltered between 0.8 and 4.5 Hz. This plot should give us an idea about the frequency range where we would expect the highest signal amplitudes.

The lower part of the figure shows the number of observations in each distance bin.

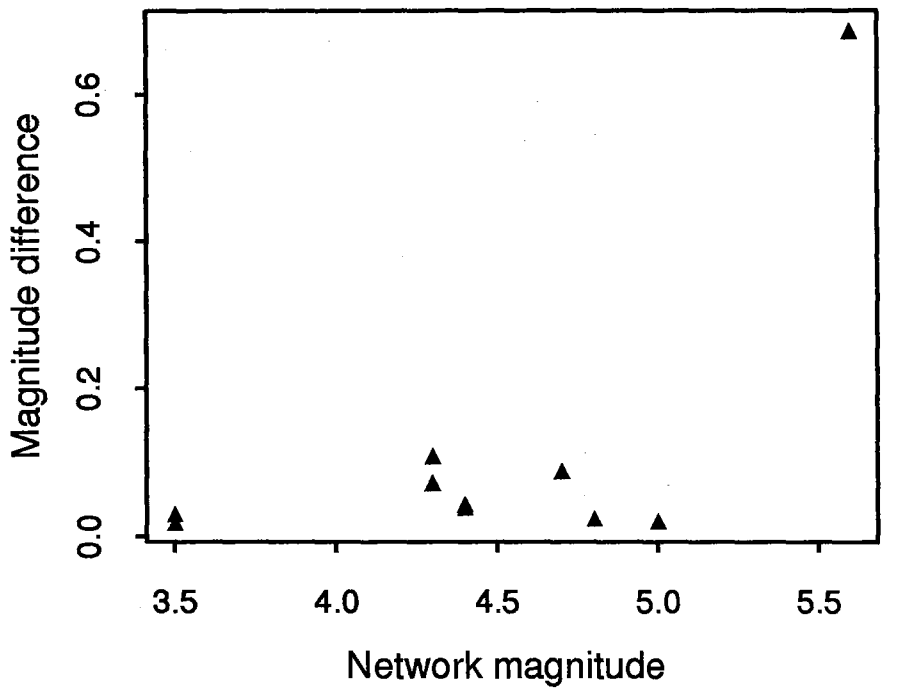

Fig. 7.3.4. For the 10 **ASAR** *events given in Table 7.3.1, we have manually measured the maximum A/T (amplitude and period) on both unfiltered and filtered (0.8-4.5 Hz) data. The magnitude difference, $log(A/T)_{unfiltered}$-$log(A/T)_{filtered}$, is plotted versus the network magnitude of the events. Except for the largest event of m_b 5.6, the correspondence was good, and log(A/T) was on the average about 0.05 m_b units lower after prefiltering.*

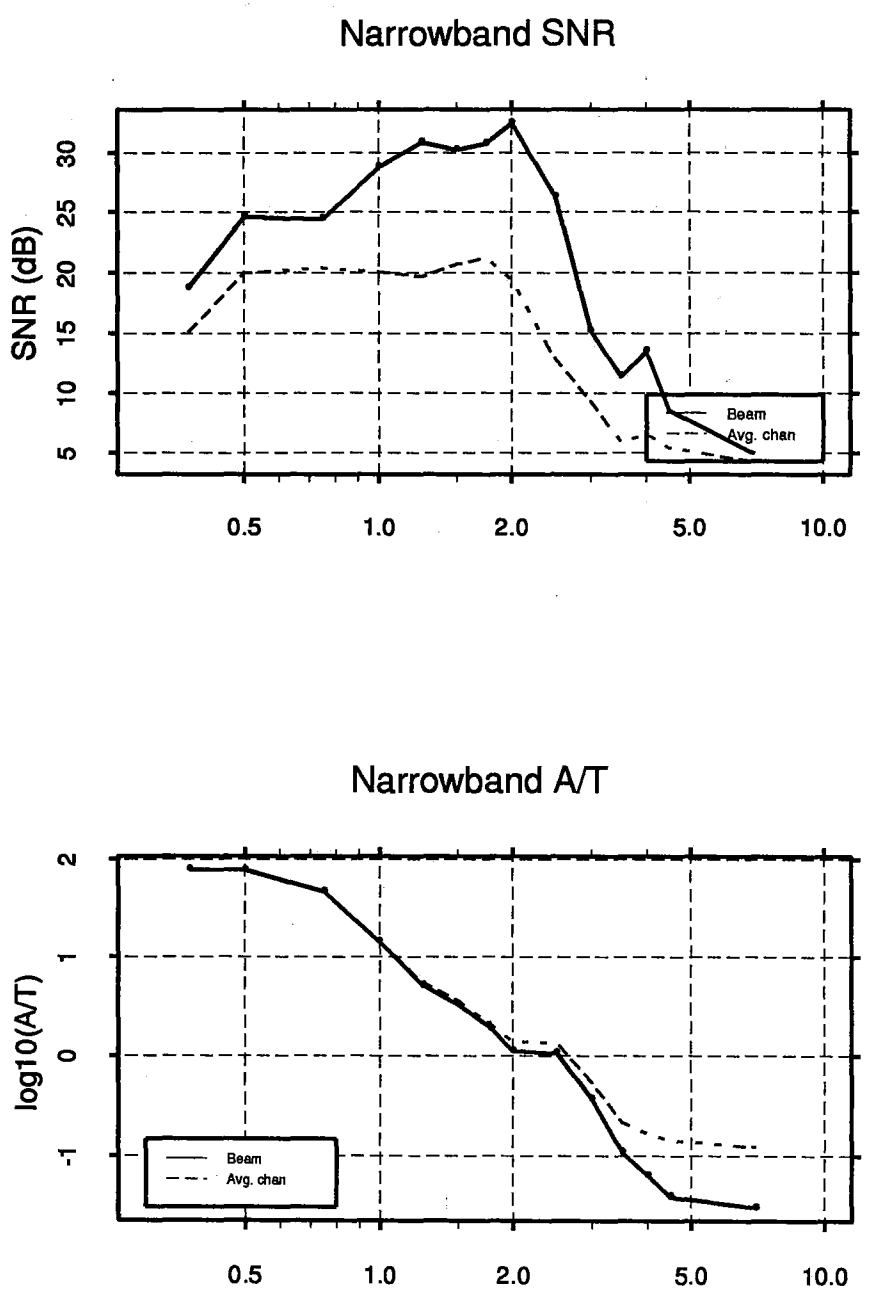

Fig. 7.3.5. Narrowband SNR and narrowband A/T for the m_b 5.6 event (event no. 9 of Table 7.3.1). For details on the plot and data analysis see Fig. 7.3.2. Notice that the largest values of log(A/T) are found for frequencies below 0.8 Hz, whereas the highest SNR is measured between 1 and 2.5 Hz.

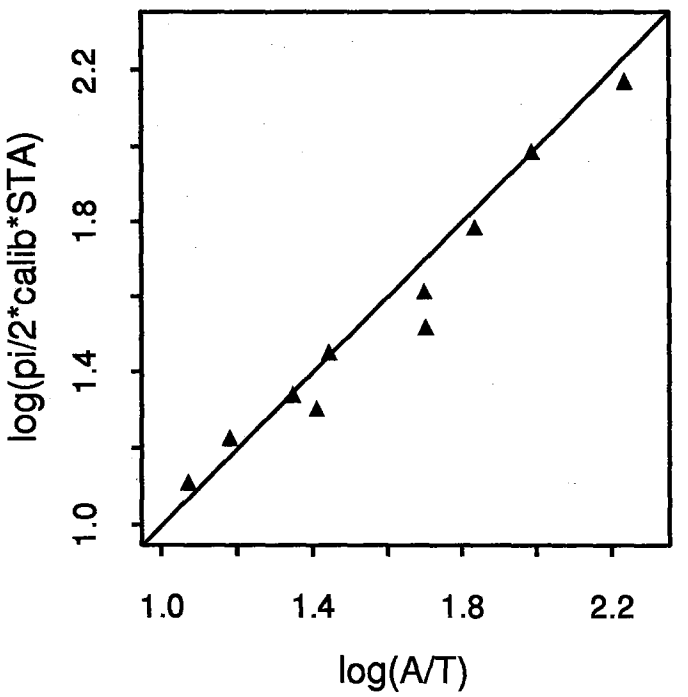

Fig. 7.3.6. This figure shows the relation between the manually measured log(A/T) values and the corresponding values of $\log(\frac{\pi}{2} \cdot calib \cdot STA)$*, where calib is the calibration constant at the reference period. log(A/T) is for this small data set 0.04 units higher than* $\log(\frac{\pi}{2} \cdot calib \cdot STA)$.

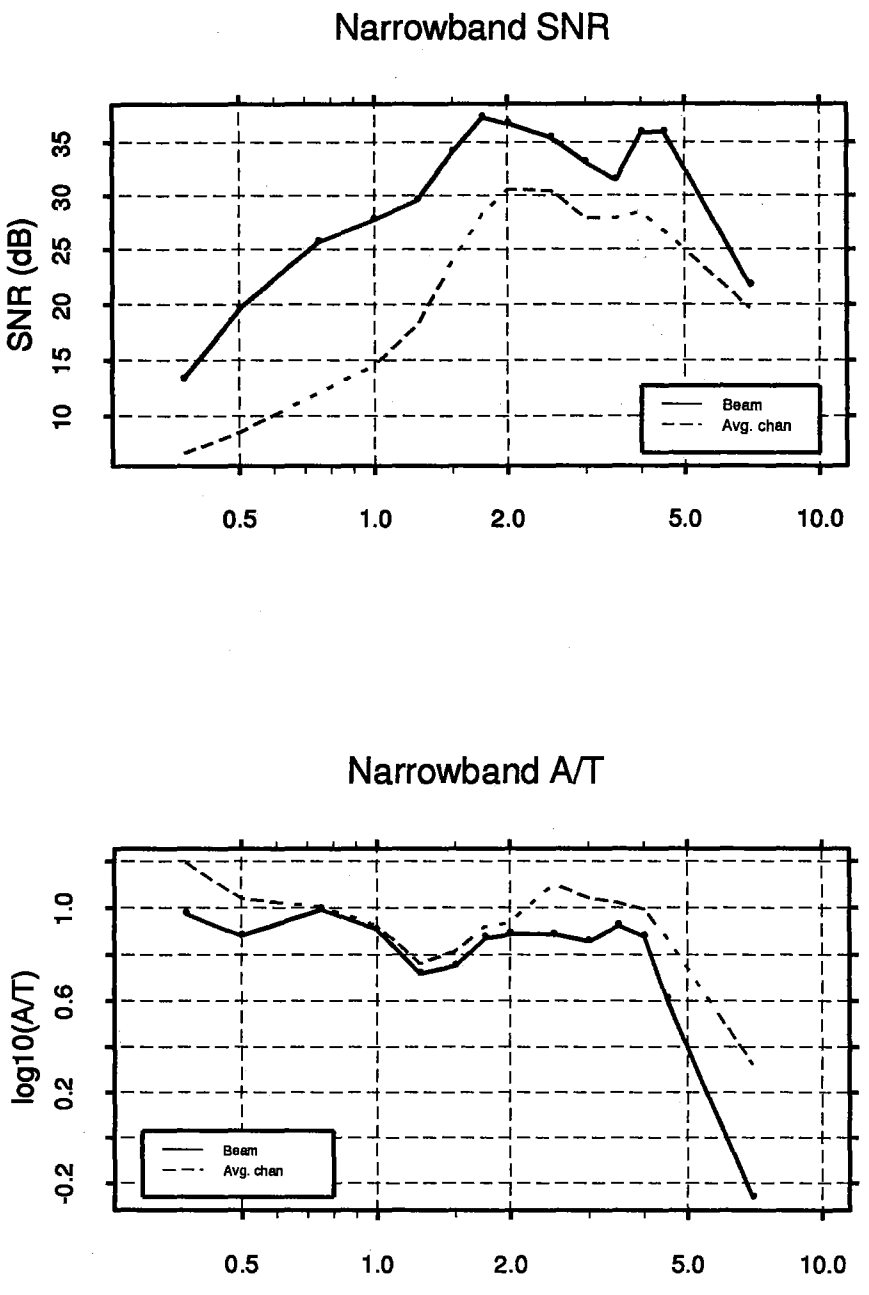

Fig. 7.3.7. Narrowband SNR and narrowband A/T for the regional event at 15.9 degrees distance (event no. 1 of Table 7.3.1). For details on the plot and data analysis see Fig. 7.3.2. Notice the relatively high signal energy up to 4 Hz, as shown on the lower panel of the plot.

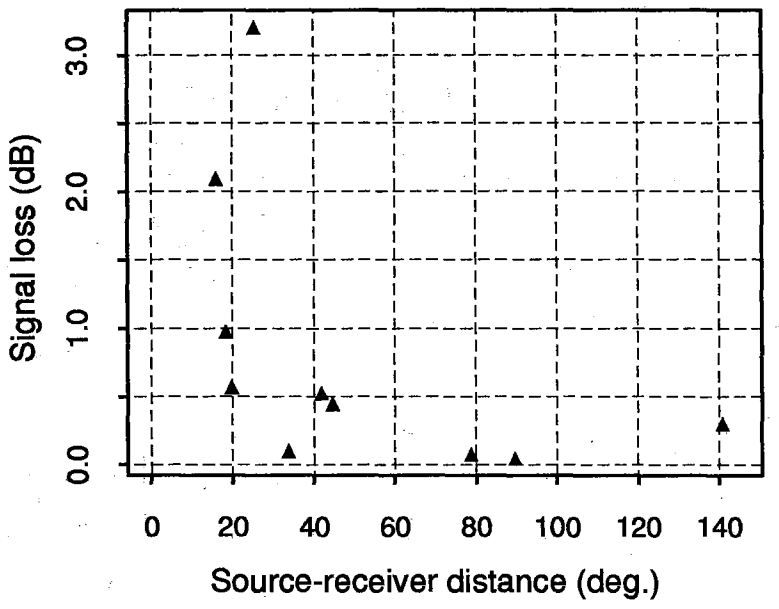

Fig. 7.3.8. Signal loss in the 0.8-4.5 Hz passband after beamforming of the 10 **ASAR** *events given in Table 7.3.1. The beamforming steering parameters are taken from f-k analysis in a 5.5 second window starting 0.5 seconds ahead of the P-phase onset.*

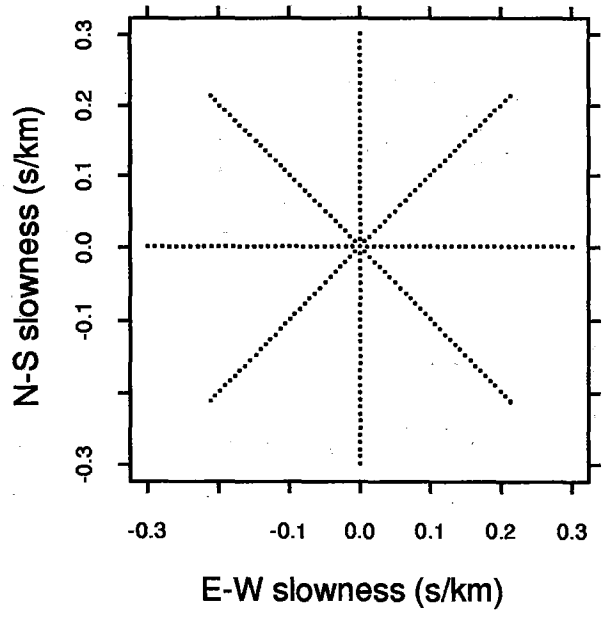

Fig. 7.3.9. This diagram represents the beamforming steering points used for the assessment of signal loss due to mis-steering of the beams. The values are relative to the observed azimuth and slowness of the events. The reason for conducting the analysis using such a pattern of steering points is to obtain representative estimates of signal loss also for arrays with a non-circular configuration like WRA and YKA.

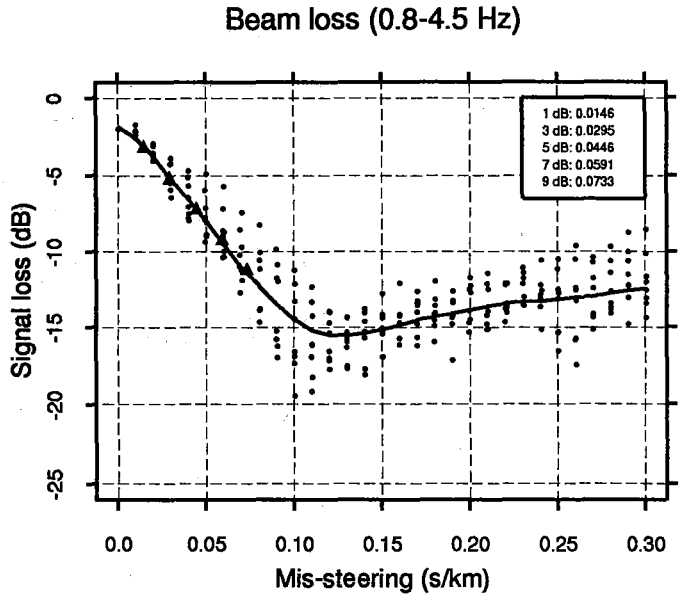

Fig. 7.3.10. Signal loss in the 0.8-4.5 Hz passband of the event at 15.9° distance (event no. 1 of Table 7.3.1) plotted as a function of the absolute value (s/km) of the mis-steering of the beams. The mis-steering points correspond to those shown in Fig. 7.3.9. The smoothed line is calculated using the S-plus function **supsmu**. *The signal loss with no mis-steering is calculated to 2.1 dB and the smoothed values of mis-steering (s/km) corresponding to additional 1, 3, 5, 7 and 9 dB signal loss are given in the legend of the figure, as well as indicated by filled triangles on the plot.*

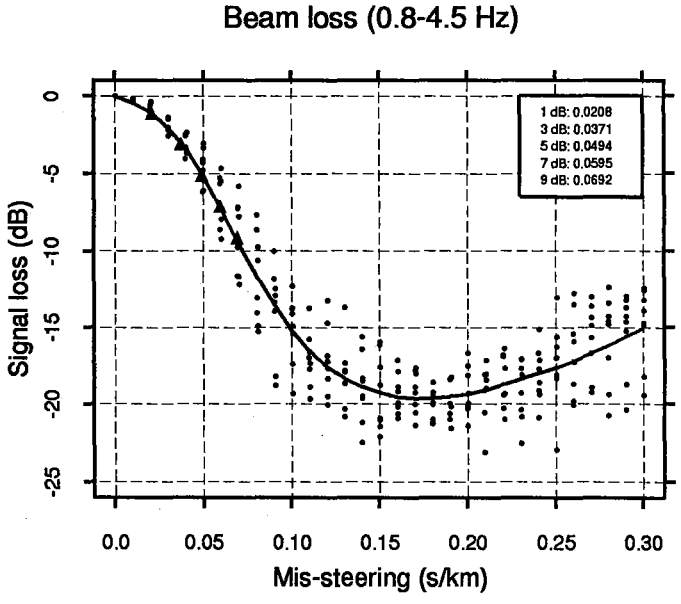

Fig. 7.3.11. Signal loss in the 0.8-4.5 Hz passband of the event at 33.6° distance (event no. 5 of Table 7.3.1) plotted as a function of the absolute value (s/km) of the mis-steering of the beams. The signal loss with no mis-steering is calculated to 0.1 dB and the smoothed values of mis-steering (s/km) corresponding to additional 1, 3, 5, 7 and 9 dB signal loss are given in the legend of the figure.

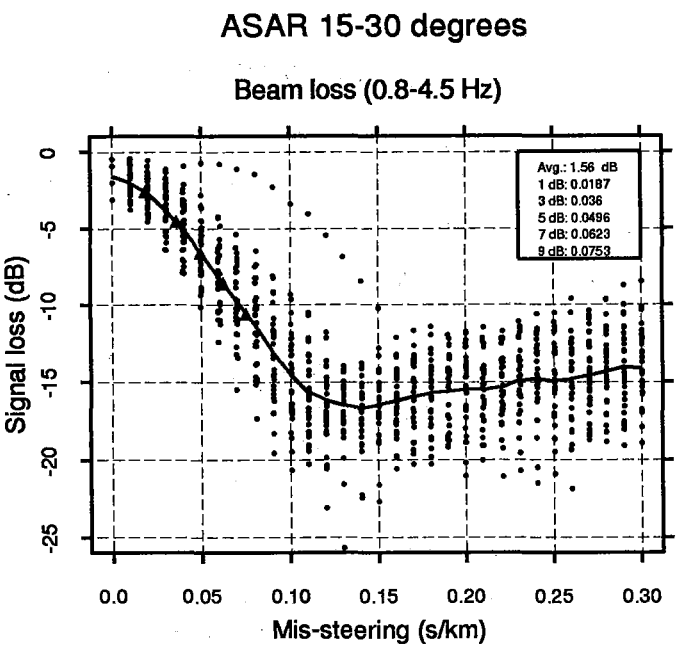

Fig. 7.3.12. Average loss in the 0.8-4.5 Hz passband of the events in the distance interval 15-30° plotted as a function of the absolute value (s/km) of the mis-steering of the beams. The smoothed estimate of signal loss with no mis-steering is calculated to 1.56 dB and the smoothed values of mis-steering (s/km) corresponding to additional 1, 3, 5, 7 and 9 dB signal loss are given in the legend of the figure.

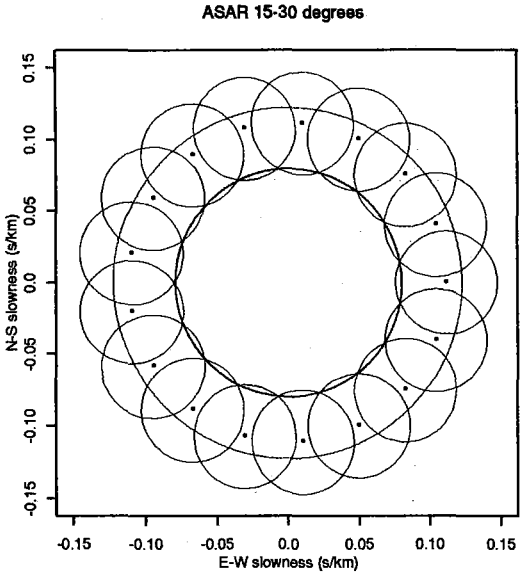

Fig. 7.3.13. Beam deployment for threshold monitoring of events between 15 and 30 degrees distance. The area between the two bold circles corresponds to the expected slowness range according to the IASP91 travel-time table for P-phases from surface events between 15 and 30 degrees. In order to ensure complete coverage within the 3 dB level, it was necessary to deploy only 12 beams. But by extending the beam deployment to 17 beams, and moving the steering points to larger slownesses, the same beam deployment could be used for processing of the 2-15 degrees interval. The steering points of the 17 beams are given by the centers of the small circles. The radii of the small circles are 0.036 s/km, corresponding to the expected mis-steering associated with the 3 dB signal loss (see Fig. 7.3.12).

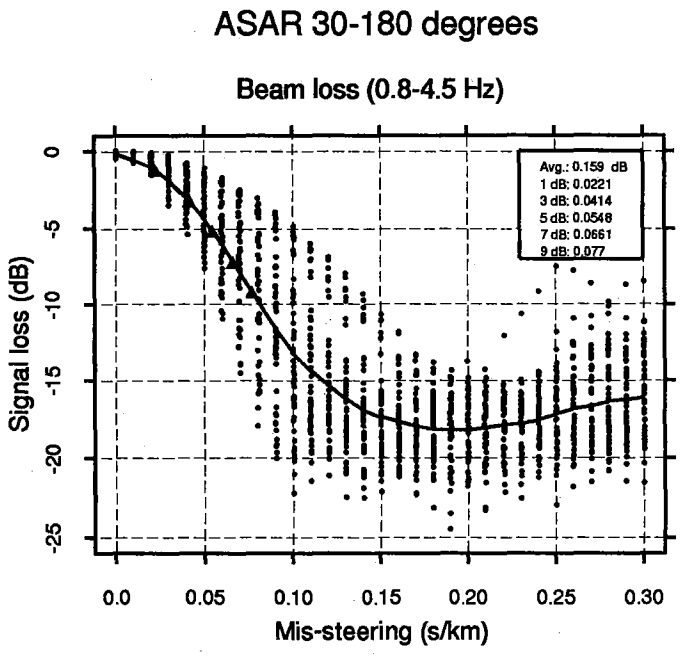

Fig. 7.3.14. Average loss in the 0.8-4.5 Hz passband of the events in the distance interval 30-180° plotted as a function of the absolute value (s/km) of the mis-steering of the beams. The signal loss with no mis-steering is calculated to 0.16 dB and the smoothed values of mis-steering (s/km) corresponding to additional 1, 3, 5, 7 and 9 dB signal loss are given in the legend of the figure.

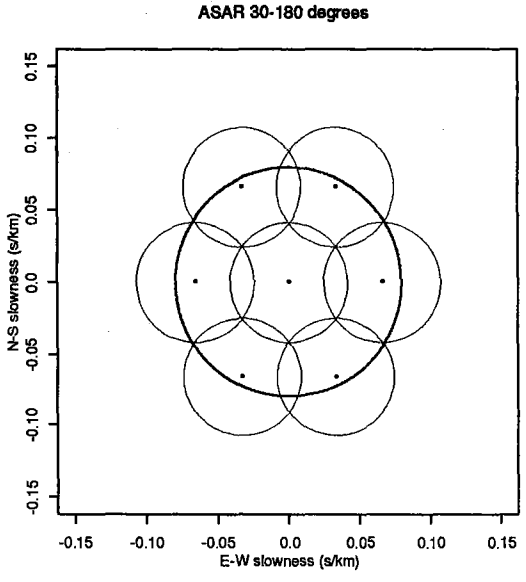

Fig. 7.3.15. Beam deployment for threshold monitoring of events in the distance interval 30-180 degrees. The area within the bold circle corresponds to the expected slowness range according to the IASP91 travel-time table for P-phases from surface events in this distance interval. In order to ensure close to complete coverage within the 3 dB level, it was necessary to deploy 7 beams, represented by the centers of the small circles. The radii of the small circles are 0.041 s/km, corresponding to the expected mis-steering associated with the 3 dB signal loss (see Fig. 7.3.14).

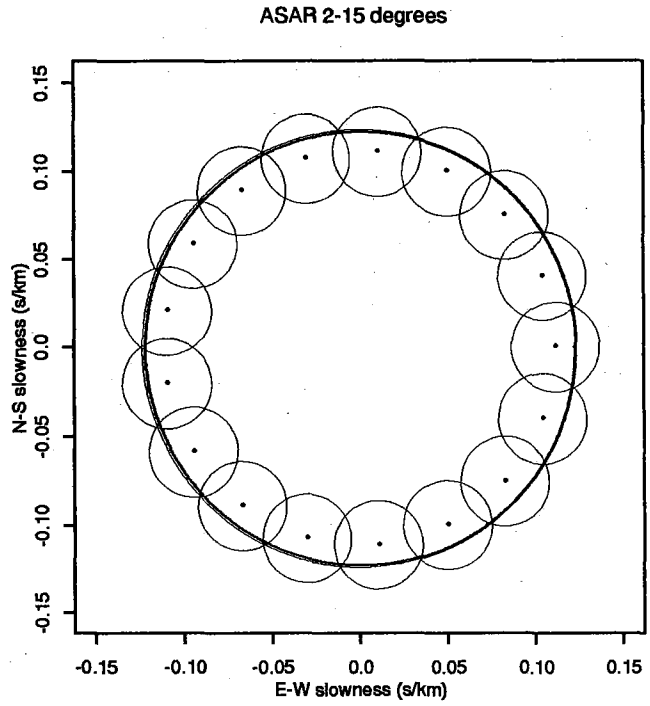

Fig. 7.3.16. Estimated beam deployment for threshold monitoring of events between 2 and 15 degrees distance, assuming a 30% increase in signal loss due to mis-steering relative to events between 15 and 30 degrees. The small area between the two bold circles corresponds to the expected slowness range according to the IASP91 travel-time table for P-phases from surface events between 2 and 15 degrees. By extending the beam deployment for the 15-30 degrees interval to 17 beams and moving the steering points to larger slowness, the same beam deployment could be used for processing of the 2-15 degrees interval. The estimated radii of the small circles are 0.025 s/km, which is 30% smaller than for events within the 15-30 degrees distance range.

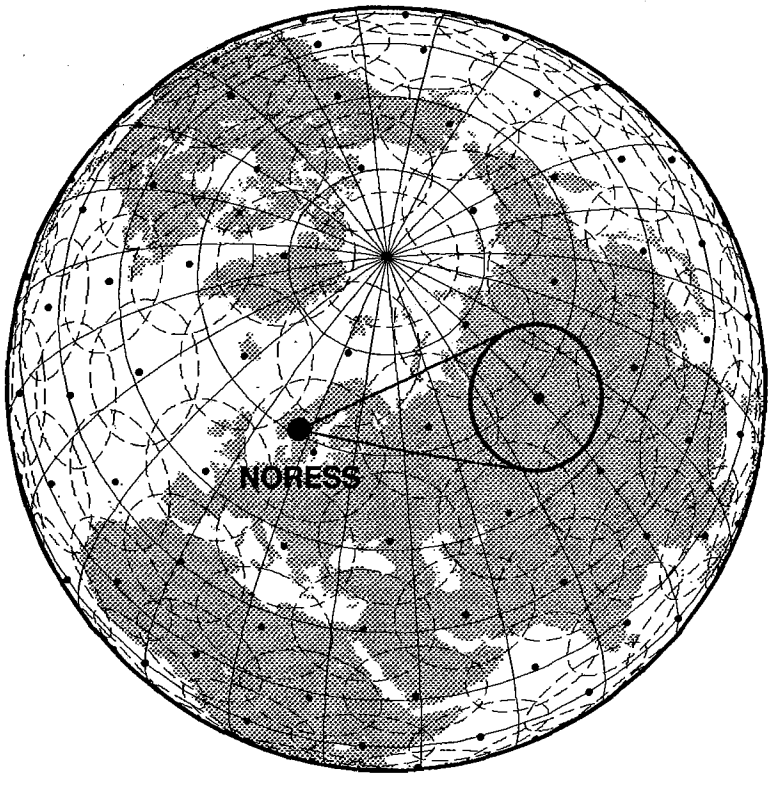

Fig. 7.3.17. Example of a global grid system for threshold monitoring. In order to ensure complete coverage of the Earth's surface, each grid point represents a circular target area. As illustrated on the figure, hypothetical events from a given target area (in this case the highlighted) will span a given range of azimuths, slowness and travel-time when recorded at a given station (in this case NORESS). If we at NORESS deploy a beam with steering parameters corresponding to the center of the highlighted target area, we will need to allow for some mis-steering to cover the entire target area. This mis-steering will generally increase with decreasing distance to the grid points. In order to obtain realistic network magnitude thresholds, the signal loss caused by this mis-steering needs to be taken into account.

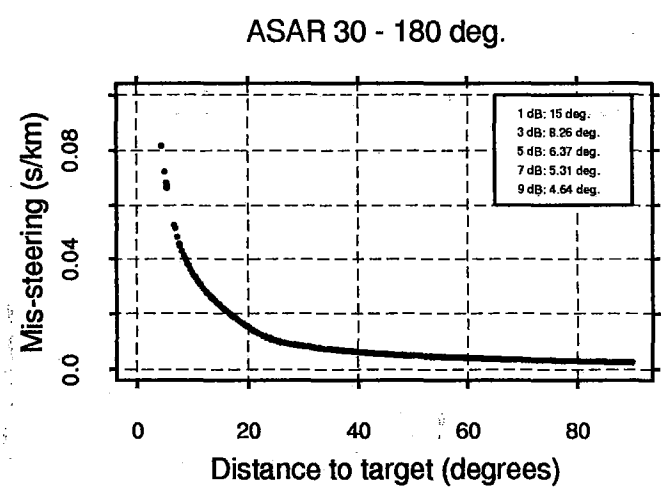

Fig. 7.3.18a. Maximum mis-steering (in s/km) associated with the 2562 globally distributed grid points used in the Threshold Monitoring at the IDC, plotted versus the distance from **ASAR** *to each of the grid points. Grid points more distant than 90 degrees have not been plotted. The legend provides information on the station-target distances for which the mis-steering causes 1, 3, 5, 7 and 9 dB signal loss when using the relation between signal loss and mis-steering representative for events between 30 and 180 degrees (see Fig. 7.3.14). Notice that for distance above 30 degrees, the mis-steering necessary to compensate for the area of the target regions causes significantly less than 1 dB signal loss.*

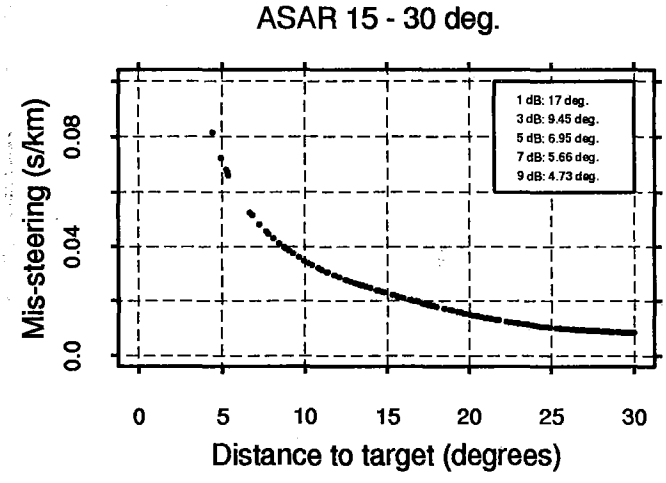

Fig. 7.3.18b. Same as Fig. 7.3.18a, but now for grid points between 15 and 30 degrees. For information on the relation between mis-steering and signal loss, see Fig. 7.3.12. Notice that for the distance interval under discussion (15-30 degrees), the mis-steering necessary to compensate for the area of the target regions causes 1 dB signal loss at 17 degrees distance, and about 1.5 dB at 15 degrees.

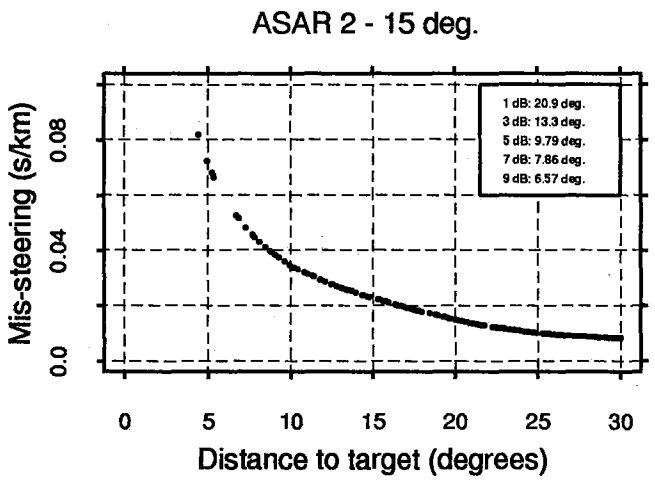

Fig. 7.3.18c. Same as Fig. 7.3.18a, but now for grid points between 2 and 15 degrees. The basis for the relation between mis-steering and signal loss are the values derived for events between 15 and 30 degrees, see Fig. 7.3.12, but now assuming a 30% increase in the sensitivity to mis-steering. Under this assumption we read from the legend that for the distance interval under discussion (2-15 degrees), the mis-steering necessary to compensate for the area of the target regions causes 3 dB signal loss at 13.3 degrees, 5 dB at 9.8 degrees, 7 dB at 7.9 degrees and 9 dB at 6.6 degrees.